Two-Degree-of-Freedom Active Disturbance Rejection Current Control for Permanent Magnet Synchronous Motors

Shiyu Lin, *Student Member, IEEE*, Yanfei Cao, *Member, IEEE*, Chen Li, Zhiqiang Wang, *Member, IEEE*, Tingna Shi, *Member, IEEE*, and Changliang Xia, *Senior Member, IEEE*

***Abstract*—In the control of permanent magnet synchronous motors, the active disturbance rejection control (ADRC) has attracted considerable attention due to its intrinsic ability for disturbance rejection. However, the existing ADRC methods have the problem of coupling the reference tracking performance and disturbance suppression performance. To simultaneously improve the current control's dynamic response speed and steady-state control accuracy, a two-degree-of-freedom ADRC current control method based on the improved extended state observer (IESO) is proposed in this article. First, the designed IESO cancels the error correction term in the observed current update law to realize the complete decoupling of the reference tracking performance and disturbance suppression performance. Under the decoupling structure, the observed disturbance update law of the IESO is designed as a proportional-integral-repetitive control structure to suppress periodic and aperiodic disturbances. Then, the system stability is proved by analyzing the distribution of characteristic roots, and a two-step parameter tuning guideline of the IESO is provided. The proposed method realizes the complete decoupling of the reference tracking performance and disturbance suppression performance, reducing the complexity of the controller parameter selection and facilitating the realization of the high-performance current control. Finally, the effectiveness of the proposed method is validated by experimental results.**

***Index Terms*—Active disturbance rejection control (ADRC), current control, permanent magnet synchronous motor (PMSM), two-degree-of-freedom controller.**

Manuscript received 15 September 2022; accepted 2 November 2022. Date of publication 8 November 2022; date of current version 26 December 2022. This work was supported in part by the Major Program of National Natural Science Foundation of China under Grant 51991384 and in part by the National Natural Science Foundation of China under Grant 51977150. Recommended for publication by Associate Editor L. V. Iyer. *(Corresponding authors: Yanfei Cao; Changliang Xia.)*

Shiyu Lin, Yanfei Cao, Chen Li, and Tingna Shi are with the College of Electrical Engineering, Zhejiang University, Hangzhou 310027, China, and also with the Zhejiang University Advanced Electrical Equipment Innovation Center, Hangzhou 311107, China (e-mail: linshiyu@zju.edu.cn; caoyanfei@zju.edu.cn; lich@tju.edu.cn; tnshi@zju.edu.cn).

Zhiqiang Wang is with the School of Electrical Engineering, Tiangong University, Tianjin 300387, China (e-mail: wangzhiqiang@tiangong.edu.cn).

Changliang Xia is with the School of Electrical Engineering, Tiangong University, Tianjin 300387, China, and also with the College of Electrical Engineering, Zhejiang University, Hangzhou 310027, China (e-mail: motor@tju.edu.cn).

Color versions of one or more figures in this article are available at https://doi.org/10.1109/TPEL.2022.3220565.

Digital Object Identifier 10.1109/TPEL.2022.3220565

NOMENCLATURE

i_{d}, i_{q}	d- and q-axes stator currents.
u_{dref}, u_{qref}	Output reference voltages of d- and q-axes current controllers.
L_{d}, L_{q}	d- and q-axes stator inductances.
L_{dn}, L_{qn}	Nominal values of d- and q-axes stator inductances.
ΔL_{d}, ΔL_{q}	Deviation values of d- and q-axes stator inductances.
ψ_{rd}, ψ_{rq}	d- and q-axes permanent magnet fluxes.
$\psi_{\mathrm{rd}6n}$, $\psi_{\mathrm{rq}6n}$	d- and q-axes $6n$th ($n = 1, 2, 3\ldots$) permanent magnet flux harmonics, whose fundamental frequency is the electrical angular frequency.
Δu_{d}, Δu_{q}	d- and q-axes $6n$th voltage harmonics, caused by the deadtime effect of the inverter.
d_{d}, d_{q}	d- and q-axes lumped disturbances.
T_{s}, T_{d}	Sampling period and deadtime.
$\hat{\boldsymbol{i}}$, $\hat{\boldsymbol{d}}$	Observed values of the current and lumped disturbance.
p	$\mathrm{p} = \mathrm{d}/\mathrm{d}t$ is the differentiation operator.
R	Stator resistance.
ω_{e}	Electrical angular speed.
ψ_{rd0}	DC component of the d-axis permanent magnet flux.
U_{dc}	DC-link voltage.
k_{p}	Proportional gain of the control law.
h_1, h_2	Gains of the observer.
ω_{o}	Bandwidth of the observer.
$G_{\mathrm{t}}(z)$	Transfer function, which characterizes the reference tracking performance of the discrete-time closed-loop system.
$G_{\mathrm{d}}(z)$	Transfer function, which characterizes the disturbance rejection performance of the discrete-time closed-loop system.
$G_{\mathrm{rc}}(z)$	Discrete-time repetitive controller.
k_{rc}	Proportional gain of the repetitive controller.
Q	Feedback gain of the repetitive controller.
K	Number of sampling period delay compensation of the repetitive controller.
N	Number of sampling period delay of the repetitive controller; $N = [\omega_{\mathrm{s}}/\omega_{\mathrm{d}}]$, where ω_{s} and ω_{d} are the sampling frequency and disturbance frequency,

respectively; $\omega_{\mathrm{d}} = 6\omega_{\mathrm{e}}$ is chosen to calculate the N online.

I. Introduction

PERMANENT magnet synchronous motors (PMSMs) have been widely used in industrial applications because of their high power density, high reliability, and good dynamic performance [1]. A field-oriented-control-based multiloop cascade control scheme is usually adopted for PMSM drives [2]. As the innermost loop, the control performance of the current loop directly determines the control performance of the torque and further the control performances of the speed and position. Therefore, the current control with high dynamic response and steady-state accuracy is the key to achieving the excellent operation performance of PMSM drive systems [3].

However, the multivariable nonlinear coupling model of the PMSM, as well as various disturbances existing in the system, increase the difficulty of realizing the high-performance current control [4]. In recent years, the active disturbance rejection control (ADRC) has attracted considerable attention in PMSM drives due to its intrinsic disturbance rejection ability and model-free characteristic. The ADRC was first proposed by Han in 1998 [5], aiming to develop an alternative practical control method to the classical proportional-integral-derivative method [6]. As the core part of the ADRC, the extended state observer (ESO) can unify internal and external disturbances as lumped disturbances for the observation and feedforward compensation, thereby improving the disturbance suppression performance of the system. The original ADRC adopts the nonlinear ESO to achieve good disturbance rejection [7]. However, the complex gain design and stability proof of the nonlinear ESO make the original ADRC somewhat tricky to implement [8]. Aiming to address the problems, Gao [9] proposed the linear ADRC by replacing the nonlinear ESO with the linear ESO. The linear ADRC has not only the simple gain design and stability proof [10], but also better control performance when disturbances are large [11], [12], which makes it more widely employed in PMSM drives [13], [14], [15], [16]. In [15], an enhanced linear ADRC current control method considering the effects of the high operating speed, modulation, and computational delays is proposed to improve the robustness of PMSM drives to internal and external disturbances at a low sampling ratio. In [16], an active-disturbance-rejection-based sliding mode current controller is proposed to improve the immunity of the current control to parameter variations and model uncertainties, thereby enhancing the current's steady-state and transient tracking performance.

The ADRC has a good suppression performance for aperiodic disturbances such as parameter variations or mismatches. However, there are not only aperiodic disturbances in the current loop of PMSM drives but also periodic disturbances mainly caused by the permanent magnet flux harmonics and the deadtime effect of the inverter [17], [18]. If these periodic disturbances are not rejected by specific methods, they will result in a significant current oscillation and deteriorate the control performance of PMSM drives [19]. Unfortunately, the conventional ADRC cannot effectively suppress these periodic disturbances due to the limited observation bandwidth of the ESO for disturbances [20]. According to the internal model principle, scholars propose a class of composite ADRC methods based on the improved control law to address this problem. The composite methods embed a type of controller that can suppress periodic disturbances, such as the repetitive controller, resonant controller, etc., into the control law of the conventional ADRC [21], [22], [23]. In [22], a discrete-time repetitive control-based ADRC current control method is proposed to improve the steady-state control accuracy of the current. In this method, the output of the repetitive controller is used to compensate for periodic disturbances, and the output of the ESO is used to compensate for aperiodic disturbances. In [23], a current control method combining a vector resonant controller and an ADRC controller is proposed to suppress periodic and aperiodic disturbances simultaneously to reduce the harmonic contents of phase currents. However, those mentioned above composite ADRC controllers belong to the one-degree-of-freedom type. The reference tracking performance and disturbance rejection performance of the system are coupled. Although the composite methods can enhance the suppression performance for periodic disturbances, they may deteriorate the tracking performance for reference commands to a certain extent. In practical applications, a tradeoff between two performances is needed, making the controller parameter tuning cumbersome and challenging to simultaneously achieve the current control with high dynamic response and high steady-state accuracy.

In order to achieve the complete decoupling of the system's reference tracking performance and disturbance suppression performance based on simultaneously suppressing periodic and aperiodic disturbances in the current loop, a two-degree-of-freedom ADRC current control method based on the improved ESO (IESO) is proposed in this article. Unlike the indirect idea of optimizing the control law for existing composite methods, the proposed method directly modifies the structure of the conventional ESO. In order to achieve the complete decoupling of the reference tracking performance and disturbance rejection performance, the designed IESO cancels the error correction term in the observed current update law of the conventional ESO. Under this decoupling structure, to realize the simultaneous suppression of periodic and aperiodic disturbances in the current loop, the observed disturbance update law of the IESO is designed as a proportional-integral-repetitive control structure. Compared with the existing related works, the main contributions and advantages of the proposed method are summarized as follows.

1) The proposed method can simultaneously improve the reference tracking performance and disturbance rejection performance by tuning the controller's parameters. It is advantageous to realize the current control with high dynamic response and high steady-state accuracy.
2) Since the reference tracking performance and the disturbance rejection performance are fully decoupled, in practical applications, there is no need to make tradeoffs between these two performances, making the controller parameter tuning simple. In addition, a two-step parameter

tuning guideline of the IESO is provided to further reduce the complexity of the controller parameter tuning.

3) Compared with the existing ADRC current control methods, the proposed method has a better control performance for tracking the reference commands and suppressing periodic and aperiodic disturbances.

The rest of this article is organized as follows. In Section II, the mathematical model of the PMSM considering disturbances is remodeled to reduce the model complexity by taking advantage of the model-free characteristic of the ADRC. In Section III, the coupling characteristic of the existing ADRC methods is analyzed. In Section IV, the proposed two-degree-of-freedom ADRC current control method is introduced; the decoupling characteristic, stability, and control performance of the proposed method are analyzed in detail in the discrete-time domain; the two-step parameter tuning guideline of the IESO is provided. Finally, the comparative experiments are implemented to verify the effectiveness of the proposed method in Section V, and Section VI concludes this article.

II. Mathematical Model of PMSM Considering Disturbances

In the synchronously rotating coordinate, the mathematical model of the PMSM, considering the deadtime effect of the inverter and permanent magnet flux harmonics, can be expressed as

$$\begin{cases} \mathrm{p}i_\mathrm{d} = L_\mathrm{d}^{-1}\left[u_\mathrm{dref} - Ri_\mathrm{d} + \omega_\mathrm{e}\left(L_\mathrm{q}i_\mathrm{q} + \psi_\mathrm{rq}\right) + \Delta u_\mathrm{d}\right] \\ \mathrm{p}i_\mathrm{q} = L_\mathrm{q}^{-1}\left[u_\mathrm{qref} - Ri_\mathrm{q} - \omega_\mathrm{e}\left(L_\mathrm{d}i_\mathrm{d} + \psi_\mathrm{rd}\right) + \Delta u_\mathrm{q}\right] \end{cases} \tag{1}$$

where

$$\begin{cases} \psi_\mathrm{rd} = \psi_\mathrm{rd0} + \sum_{n=1}^{\infty} \psi_\mathrm{rd6}n \cos\left(6n\omega_\mathrm{e}t\right) \\ \psi_\mathrm{rq} = \sum_{n=1}^{\infty} \psi_\mathrm{rq6}n \sin\left(6n\omega_\mathrm{e}t\right) \end{cases} \tag{2}$$

$$\begin{cases} \Delta u_\mathrm{d} = \dfrac{4T_\mathrm{d}U_\mathrm{dc}}{\pi T_\mathrm{s}} \sum_{n=1}^{\infty} \left[\dfrac{12n}{36n^2-1} \sin\left(6n\omega_\mathrm{e}t\right)\right] \\ \Delta u_\mathrm{q} = \dfrac{4T_\mathrm{d}U_\mathrm{dc}}{\pi T_\mathrm{s}} \left\{-1 + \sum_{n=1}^{\infty} \left[\dfrac{2}{36n^2-1} \cos\left(6n\omega_\mathrm{e}t\right)\right]\right\} \end{cases}. \tag{3}$$

According to (1)–(3), it can be seen that PMSM drive systems contain two types of disturbances: periodic and aperiodic. Periodic disturbances are mainly caused by flux harmonics and the deadtime effect. Aperiodic disturbances are mainly caused by the stator resistance voltage drop, cross-coupling terms, and the inductance mismatches. The disturbances mentioned above are unified as lumped disturbances d_d and d_q, whose expressions are

$$\begin{cases} d_\mathrm{d} = \dfrac{\omega_\mathrm{e}\left(L_\mathrm{q}i_\mathrm{q} + \psi_\mathrm{rq}\right) + \Delta u_\mathrm{d} - Ri_\mathrm{d}}{L_\mathrm{d}} - \dfrac{\Delta L_\mathrm{d}}{L_\mathrm{dn}L_\mathrm{d}} u_\mathrm{dref} \\ d_\mathrm{q} = \dfrac{-\omega_\mathrm{e}\left(L_\mathrm{d}i_\mathrm{d} + \psi_\mathrm{rd}\right) + \Delta u_\mathrm{q} - Ri_\mathrm{q}}{L_\mathrm{q}} - \dfrac{\Delta L_\mathrm{q}}{L_\mathrm{qn}L_\mathrm{q}} u_\mathrm{qref} \end{cases}. \tag{4}$$

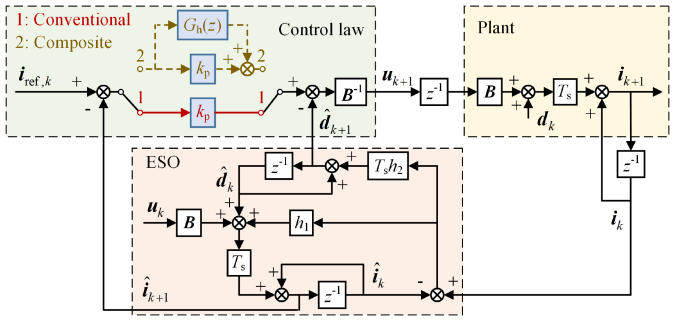

Fig. 1. Block diagrams of the conventional ADRC and composite ADRC current control.

According to (4), (1) can be rewritten as

$$\mathrm{p}\boldsymbol{i} = \boldsymbol{B}\boldsymbol{u} + \boldsymbol{d} \tag{5}$$

where $\boldsymbol{i} = [i_\mathrm{d} \quad i_\mathrm{q}]^\mathrm{T}$; $\boldsymbol{B} = \mathrm{diag}(L_\mathrm{dn}^{-1}, L_\mathrm{qn}^{-1})$; $\boldsymbol{u} = [u_\mathrm{dref} \quad u_\mathrm{qref}]^\mathrm{T}$; $\boldsymbol{d} = [d_\mathrm{d} \quad d_\mathrm{q}]^\mathrm{T}$.

By taking the first Taylor expansion, (5) is discretized in the z-domain as

$$\boldsymbol{i}_{k+1}(z) = \boldsymbol{i}_k(z) + T_\mathrm{s}\boldsymbol{B}\boldsymbol{u}_k(z) + T_\mathrm{s}\boldsymbol{d}_k(z). \tag{6}$$

III. Analysis of Coupling Characteristic of Existing ADRC Methods

The ADRC is mainly composed of the control law and ESO. Due to the limited observation bandwidth of the ESO, the conventional ADRC can suppress only aperiodic disturbances of the system but not periodic disturbances [20]. To suppress these two types of disturbances simultaneously, scholars have proposed a class of composite ADRC methods based on the improved control law. Fig. 1 shows the current control block diagrams of the conventional ADRC and the composite ADRC, in which Terminal 1 and Terminal 2 correspond to the conventional proportional control law and the composite control law, respectively.

As can be seen from Fig. 1, the composite ADRC current controller and the conventional ADRC current controller have the same ESO, except that the control laws are different. The composite ADRC combines the proportional coefficient k_p and the embedded controller $G_\mathrm{h}(z)$ parallel to form a compound control law. $G_\mathrm{h}(z)$ is the type of controller that can achieve good tracking for a set of periodic reference inputs, such as the repetitive controller and vector resonance controller. In the composite method, the output of the controller $G_\mathrm{h}(z)$ is used to compensate for periodic disturbances, while the output of the conventional ESO is used to compensate for aperiodic disturbances.

According to Fig. 1, the expressions of transfer functions $G_\mathrm{t}(z)$ and $G_\mathrm{d}(z)$, which characterize the reference tracking performance and disturbance rejection performance of the system, are (7) and (8), respectively, shown at the bottom of the next page, where $G_\mathrm{c}(z) = k_\mathrm{p}$ for the conventional ADRC; $G_\mathrm{c}(z) = k_\mathrm{p} + G_\mathrm{h}(z)$ for the composite ADRC. Ideally, $|G_\mathrm{t}(z)| \to 1$ and $|G_\mathrm{d}(z)| \to 0$.

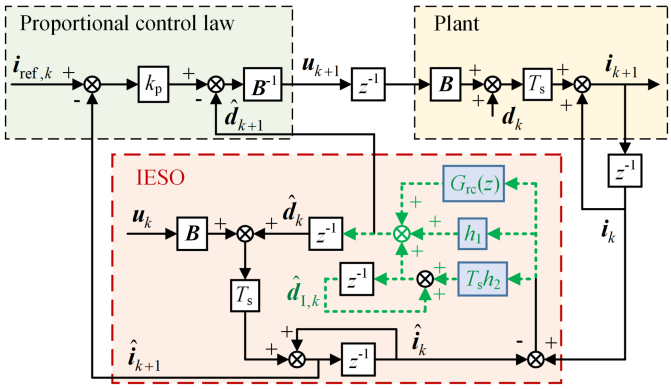

Fig. 2. Block diagram of the proposed two-degree-of-freedom ADRC current control.

According to (7) and (8), it can be seen that both transfer functions $G_t(z)$ and $G_d(z)$ contain parameters h_1, h_2, and $G_c(z)$. It indicates that the reference tracking and disturbance rejection performances are affected by the same parameters, so these two performances are fully coupled.

The disadvantages of the coupling characteristic are the following. 1) It is difficult to improve the reference tracking performance and disturbance suppression performance simultaneously. 2) In practical applications, a tradeoff between these two performances is needed, which makes the parameter tuning of the controller cumbersome.

IV. Proposed Two-Degree-of-Freedom ADRC

To fully decouple the system's reference tracking performance and disturbance rejection performance, a two-degree-of-freedom ADRC current method based on the improved ESO (IESO) is proposed, whose block diagram is shown in Fig. 2. The proposed method can simultaneously optimize the reference tracking performance and disturbance rejection performance by tuning the controller parameters, which is advantageous to realize the current control with high dynamic response and high steady-state accuracy.

A. Design of Improved ESO

The fundamental reason why the conventional ADRC cannot suppress periodic disturbances is that the disturbance observation bandwidth of the conventional ESO is limited. Therefore, unlike the existing composite method, which adopts the indirect idea of "patching" the control law, the proposed method directly modifies the structure of the conventional ESO so that the output of the observer can compensate for periodic and aperiodic disturbances at the same time. The expression of the designed IESO is

$$\begin{cases} \hat{\boldsymbol{i}}_{k+1}(z) = \hat{\boldsymbol{i}}_k(z) + T_s\boldsymbol{B}\boldsymbol{u}_k(z) + T_s\hat{\boldsymbol{d}}_k(z) \\ \hat{\boldsymbol{d}}_{k+1}(z) = \hat{\boldsymbol{d}}_{I,k+1}(z) + [h_1 + G_{rc}(z)]\,[\boldsymbol{i}_k(z) - \hat{\boldsymbol{i}}_k(z)] \\ \hat{\boldsymbol{d}}_{I,k+1}(z) = \hat{\boldsymbol{d}}_{I,k}(z) + T_s h_2[\boldsymbol{i}_k(z) - \hat{\boldsymbol{i}}_k(z)] \end{cases} \tag{9}$$

where $\hat{\boldsymbol{d}}_{I,k}(z)$ is the integral component of the observed lumped disturbance $\hat{\boldsymbol{d}}_k(z)$; $G_{rc}(z)$ is the discrete-time repetitive controller [22], whose expression is

$$G_{rc}(z) = \frac{k_{rc}z^{-N+K}}{1 - Qz^{-N}}. \tag{10}$$

According to Fig. 1, the expression of the conventional ESO is

$$\begin{cases} \hat{\boldsymbol{i}}_{k+1}(z) = \hat{\boldsymbol{i}}_k(z) + T_s\{\boldsymbol{B}\boldsymbol{u}_k(z) + \hat{\boldsymbol{d}}_k(z) \\ \quad + h_1[\boldsymbol{i}_k(z) - \hat{\boldsymbol{i}}_k(z)]\} \\ \hat{\boldsymbol{d}}_{k+1}(z) = \hat{\boldsymbol{d}}_k(z) + T_s h_2[\boldsymbol{i}_k(z) - \hat{\boldsymbol{i}}_k(z)]. \end{cases} \tag{11}$$

By comparing (9) and (11), as well as block diagrams of the observers in Figs. 1 and 2, the differences between the designed IESO and the conventional ESO are as follows.

1) To fully decouple the reference tracking performance and disturbance suppression performance, the designed IESO cancels the error correction term $h_1[\boldsymbol{i}_k(z) - \hat{\boldsymbol{i}}_k(z)]$ in the update law of the observed current $\hat{\boldsymbol{i}}_{k+1}(z)$.
2) To simultaneously suppress periodic and aperiodic disturbances in the current loop, under the decoupling structure, the update law of the observed disturbance $\hat{\boldsymbol{d}}_{k+1}(z)$ of the IESO is designed as a proportional-integral-repetitive control structure.

B. Analysis of Decoupling Characteristic

In this section, the transfer functions of the closed-loop system are derived and analyzed to illustrate the decoupling characteristic of the proposed method.

In order to analyze the decoupling characteristic more intuitively, (9) is rewritten as

$$\begin{cases} \hat{\boldsymbol{i}}_{k+1}(z) = \hat{\boldsymbol{i}}_k(z) + T_s\boldsymbol{B}\boldsymbol{u}_k(z) + T_s\hat{\boldsymbol{d}}_k(z) \\ \hat{\boldsymbol{d}}_{k+1}(z) = G_o(z)[\boldsymbol{i}_k(z) - \hat{\boldsymbol{i}}_k(z)] \end{cases} \tag{12}$$

$$G_t(z) = \frac{\boldsymbol{i}_{k+1}(z)}{\boldsymbol{i}_{ref,k}(z)} = \frac{[(1 - z^{-1} + T_s h_1 z^{-1})(1 - z^{-1}) + T_s^2 h_2 z^{-2}]T_s G_c(z) z^{-1}}{[1 + (T_s h_1 - 2)z^{-1} + (1 - T_s h_1 + T_s^2 h_2)z^{-2}]\{1 + [T_s G_c(z) - 1]z^{-1}\}} \tag{7}$$

$$G_d(z) = \frac{\boldsymbol{i}_{k+1}(z)}{\boldsymbol{d}_k(z)} = \frac{\{1 + [T_s G_c(z) + T_s h_1 - 1]z^{-1}\}(1 - z^{-1})T_s}{[1 + (T_s h_1 - 2)z^{-1} + (1 - T_s h_1 + T_s^2 h_2)z^{-2}]\{1 + [T_s G_c(z) - 1]z^{-1}\}}. \tag{8}$$

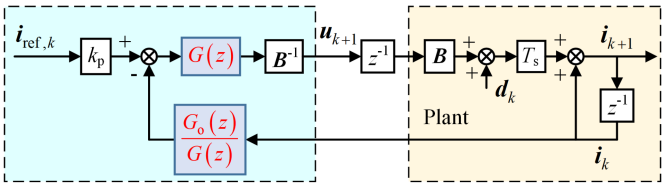

Fig. 3. Simplified block diagram of the proposed ADRC current control.

where

$$G_{\mathrm{o}}(z) = h_1 + \frac{T_{\mathrm{s}} h_2}{1 - z^{-1}} + G_{\mathrm{rc}}(z). \tag{13}$$

According to (12), $\hat{\boldsymbol{i}}_{k+1}(z)$ and $\hat{\boldsymbol{d}}_{k+1}(z)$ can be derived as

$$\begin{cases} \hat{\boldsymbol{i}}_{k+1}(z) = \dfrac{T_{\mathrm{s}}\boldsymbol{B}\boldsymbol{u}_k(z) + T_{\mathrm{s}}G_{\mathrm{o}}(z)z^{-1}\boldsymbol{i}_k(z)}{1 - z^{-1} + T_{\mathrm{s}}G_{\mathrm{o}}(z)z^{-2}} \\ \hat{\boldsymbol{d}}_{k+1}(z) = \dfrac{-T_{\mathrm{s}}\boldsymbol{B}G_{\mathrm{o}}(z)z^{-1}\boldsymbol{u}_k(z) + G_{\mathrm{o}}(z)(1-z^{-1})\boldsymbol{i}_k(z)}{1 - z^{-1} + T_{\mathrm{s}}G_{\mathrm{o}}(z)z^{-2}} \end{cases}. \tag{14}$$

According to Fig. 2, the expression of the control law of the proposed method is

$$\boldsymbol{u}_{k+1}(z) = \boldsymbol{B}^{-1}\left\{k_{\mathrm{p}}\left[\boldsymbol{i}_{\mathrm{ref},k}(z) - \hat{\boldsymbol{i}}_{k+1}(z)\right] - \hat{\boldsymbol{d}}_{k+1}(z)\right\}. \tag{15}$$

Substituting (14) into (15) yields

$$\boldsymbol{u}_{k+1}(z) = \boldsymbol{B}^{-1}G(z)\left[k_{\mathrm{p}}\boldsymbol{i}_{\mathrm{ref},k}(z) - \frac{G_{\mathrm{o}}(z)}{G(z)}\boldsymbol{i}_k(z)\right] \tag{16}$$

where

$$G(z) = \frac{1 - z^{-1} + T_{\mathrm{s}}G_{\mathrm{o}}(z)z^{-2}}{1 + (T_{\mathrm{s}}k_{\mathrm{p}} - 1)z^{-1}}. \tag{17}$$

According to (6) and (16), Fig. 2 can be reconstructed as Fig. 3. According to Fig. 3, the expressions of transfer functions $G_{\mathrm{t}}(z)$ and $G_{\mathrm{d}}(z)$ are derived as

$$G_{\mathrm{t}}(z) = \frac{\boldsymbol{i}_{k+1}(z)}{\boldsymbol{i}_{\mathrm{ref},k}(z)} = \frac{T_{\mathrm{s}}k_{\mathrm{p}}z^{-1}}{1 + (T_{\mathrm{s}}k_{\mathrm{p}} - 1)z^{-1}} \tag{18}$$

$$G_{\mathrm{d}}(z) = \frac{\boldsymbol{i}_{k+1}(z)}{\boldsymbol{d}_k(z)} = \frac{T_{\mathrm{s}}}{1 - z^{-1} + T_{\mathrm{s}}G_{\mathrm{o}}(z)z^{-2}}. \tag{19}$$

As can be seen from (18) and (19), $G_{\mathrm{t}}(z)$ only contains the parameter k_{p} of the control law, and $G_{\mathrm{d}}(z)$ only contains parameters h_1, h_2, and $G_{\mathrm{rc}}(z)$ of the IESO. It indicates that the reference tracking performance is only related to the parameter of the control law and independent of that of the IESO; the disturbance rejection performance is only related to the parameters of the IESO and independent of that of the control law. Therefore, the proposed ADRC controller is a two-degree-of-freedom controller, which fully decouples the reference tracking performance and disturbance suppression performance.

C. Stability Analysis

In this section, the system stability of the proposed method is discussed by analyzing whether the roots of the characteristic equation locate inside the unit circle. The two-step parameter tuning guideline of the IESO is proposed to reduce the complexity of the controller parameter selection.

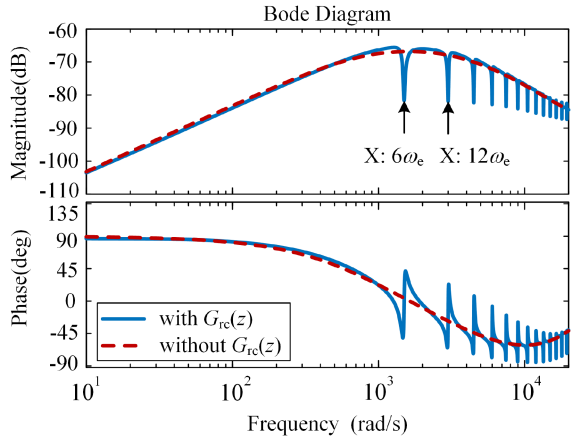

Fig. 4. Bode diagrams of the transfer functions $G_{\mathrm{d}}(z)$, where $h_1 = 2.4 \times 10^3$, $h_2 = 1.44 \times 10^6$, $k_{\mathrm{rc}} = 500$, $Q = 0.95$ and $K = 3$.

According to (18) and (19), the characteristic equation of the close-loop system is

$$\begin{cases} P(z) = P_1(z)P_2(z) = 0 \\ P_1(z) = 1 + (T_{\mathrm{s}}k_{\mathrm{p}} - 1)z^{-1} \\ P_2(z) = 1 - z^{-1} + T_{\mathrm{s}}G_{\mathrm{o}}(z)z^{-2} \end{cases}. \tag{20}$$

According to the stability criterion of the discrete-time system, if all characteristic roots of $P_1(z) = 0$ and $P_2(z) = 0$ locate inside the unit circle, the system is stable. First, the characteristic root of $P_1(z) = 0$ is

$$z = 1 - T_{\mathrm{s}}k_{\mathrm{p}}. \tag{21}$$

According to $|z| < 1$, the selection range of k_{p} ensuring the system is stable is

$$0 < k_{\mathrm{p}} < \frac{2}{T_{\mathrm{s}}}. \tag{22}$$

Then, characteristic roots of $P_2(z) = 0$ are discussed. The Bode diagrams of transfer functions $G_{\mathrm{d}}(z)$ are shown in Fig. 4. As can be seen, the repetitive controller $G_{\mathrm{rc}}(z)$ has a strong frequency selection characteristic and only affects the system's behavior within a narrow frequency band. In order to reduce the complexity of the parameter selection, the parameters of the IESO can be selected in two steps: 1) only considering the aperiodic disturbance suppression, the transfer function $G_{\mathrm{o}}(z)$ does not contain $G_{\mathrm{rc}}(z)$, and only parameters h_1 and h_2 are selected; 2) then considering the periodic disturbance suppression, $G_{\mathrm{rc}}(z)$ is added into $G_{\mathrm{o}}(z)$, and parameters k_{rc}, Q and K are selected.

1) When $G_{\mathrm{o}}(z)$ only contains h_1 and h_2, the characteristic equation $P_2(z) = 0$ can be simplified as

$$z^3 - 2z^2 + (1 + T_{\mathrm{s}}h_1 + T_{\mathrm{s}}^2h_2)z - T_{\mathrm{s}}h_1 = 0. \tag{23}$$

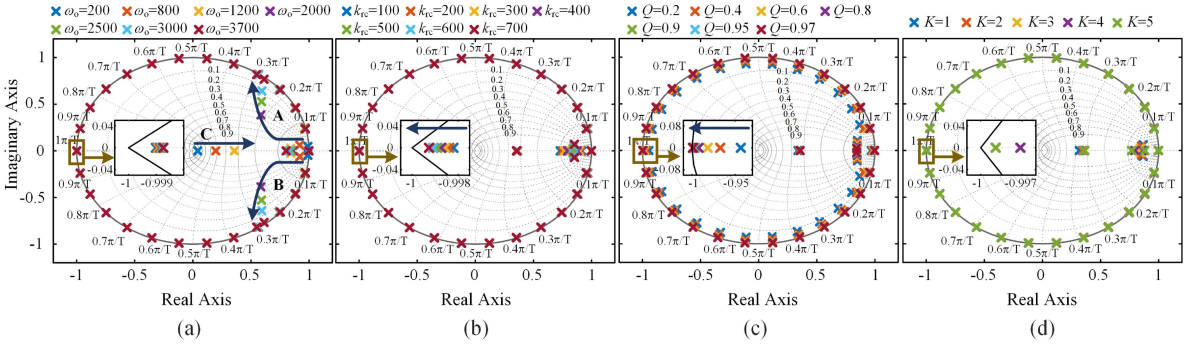

Fig. 5. Distribution law of characteristic roots of $P_2(z)=0$ with separate changes of ω_o, k_{rc}, Q, and K. (a) ω_o changes. (b) k_{rc} changes. (c) Q changes. (d) K changes.

Based on the Jury criterion [24], the condition that characteristic roots of (23) locate inside the unit circle is

$$\begin{cases} |-T_s h_1| < 1 \\ P_2(z)|_{z=1} > 0 \\ P_2(z)|_{z=-1} < 0 \\ \left|1-(T_s h_1)^2\right| > \left|1-T_s h_1+T_s^2 h_2\right| \end{cases}. \tag{24}$$

According to (24), the selection ranges of h_1 and h_2 are

$$\begin{cases} -\dfrac{1}{T_s} < h_1 < \dfrac{1}{T_s} \\ 0 < h_2 < \dfrac{h_1}{T_s} - {h_1}^2 \end{cases}. \tag{25}$$

Based on the popular bandwidth parameterization method [16], h_1 and h_2 can be designed as

$$\begin{bmatrix} h_1 & h_2 \end{bmatrix} = \begin{bmatrix} 2\omega_o & \omega_o^2 \end{bmatrix}. \tag{26}$$

According to (25), the selection range of ω_o ensuring the system is stable is

$$0 < \omega_o < \frac{2}{5T_s}. \tag{27}$$

2) When $G_o(z)$ contains $G_{rc}(z)$, h_1 and h_2, according to (13), (20), and (26), $P_2(z)=0$ can be rewritten as

$$1-z^{-1}+\left(2\omega_o+\frac{T_s\omega_o^2}{1-z^{-1}}+\frac{k_{rc}z^{-N+K}}{1-Qz^{-N}}\right)T_s z^{-2}=0. \tag{28}$$

According to (28), the distribution of characteristic roots of $P_2(z)=0$ is related to parameters ω_o, k_{rc}, Q, and K, meaning the stability is determined by the four parameters. Fig. 5 shows the distribution law of characteristic roots of $P_2(z)=0$ with separate changes of ω_o, k_{rc}, Q, and K, where $T_s=1\times10^{-4}$ s. As can be seen, when ω_o, k_{rc}, Q, and K are selected within a certain range, characteristic roots of $P_2(z)=0$ always locate inside the unit circle, and the system is stable.

Moreover, the effectiveness of the proposed two-step parameter tuning guideline of the IESO can be further validated by analyzing Fig. 5. The analysis is as follows.

1) When $G_o(z)$ only contains parameters h_1 and h_2, according to (27), the selection range of ω_o is [0, 4000]. When $G_o(z)$ contains $G_{rc}(z)$, it can be seen from Fig. 5(a) that the selection range of ω_o is [200, 3700]. Adding the repetitive controller $G_{rc}(z)$ will slightly reduce the selection range of ω_o at both ends. However, when the value of ω_o is too large or too small, the damping ratios of two poles, A and B, related to h_1 and h_2 will become small, resulting in the oscillation of the actual current. Therefore, considering the current control performance, ω_o is usually only selected in the middle range, not at both ends. Therefore, the value of ω_o selected in the first step can ensure the system is stable after $G_{rc}(z)$ is added to $G_o(z)$.
2) As can be seen from Fig. 5(a), the change of ω_o basically does not affect the distribution of poles associated with $G_{rc}(z)$ near the boundary of the unit circle, but only the distribution of three poles, A, B, and C, associated with h_1 and h_2. As can be seen from Fig. 5(b)–(d), the changes of k_{rc}, Q, and K basically do not affect the pole distribution associated with h_1 and h_2, but only the pole distribution associated with $G_{rc}(z)$. It illustrates that the effects of $G_{rc}(z)$ and ω_o on the system's stability are independent.

D. Analysis of Control Performance

In this section, the Bode diagram of the transfer function $G_d(z)$ is analyzed to illustrate that the proposed two-degree-of-freedom ADRC can effectively suppress aperiodic and periodic disturbances. In addition, the Bode diagram of the transfer function $G_t(z)$ is also analyzed to illustrate that the proposed method based on the designed IESO can track the reference command without steady-state errors.

Substituting $z=e^{j\omega_d T_s}$ into (19), the transfer function $G_d(z)$ can be expressed in the frequency domain as

$$G_d\left(e^{j\omega_d T_s}\right)=\frac{T_s}{1-e^{-j\omega_d T_s}+T_s G_o\left(e^{j\omega_d T_s}\right)e^{-2j\omega_d T_s}} \tag{29}$$

where ω_d is the disturbance frequency. The smaller $|G_d(e^{j\omega_d T_s})|$, the stronger the disturbance suppression performance.

1) Aperiodic Disturbance Suppression: During the steady-state operation of the PMSM, the frequency of aperiodic disturbances is $\omega_d=0$. Substituting $\omega_d=0$ into (29) can yield $|G_d(e^{j\omega_d T_s})|=0$, indicating that the proposed method can entirely suppress aperiodic disturbances.

2) Periodic Disturbance Suppression: According to (8) and (29), the Bode diagrams of the transfer functions $G_d(z)$ of the proposed ADRC and existing composite ADRC are shown in

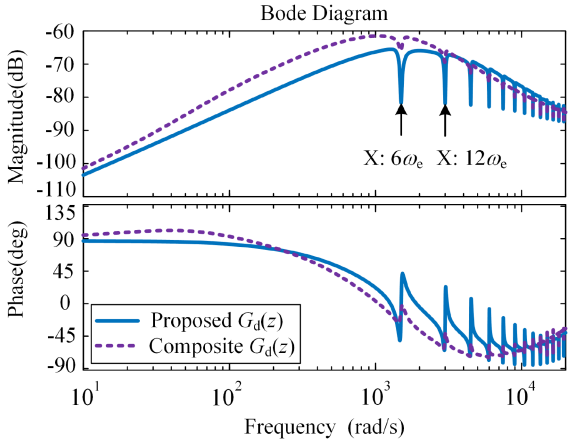

Fig. 6. Bode diagrams of the transfer functions $G_{\mathrm{d}}(z)$ of the proposed ADRC and composite ADRC, where $k_{\mathrm{p}} = 2500$, $h_1 = 2.4 \times 10^3$, $h_2 = 1.44 \times 10^6$, $k_{\mathrm{rc}} = 500$, $Q = 0.95$, and $K = 3$.

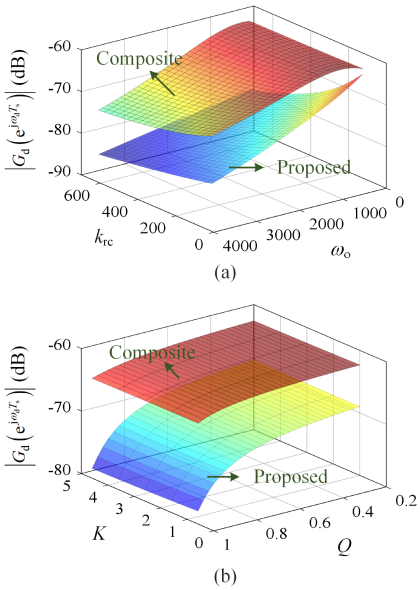

Fig. 7. Diagrams of the values of $|G_{\mathrm{d}}(\mathrm{e}^{\mathrm{j}\omega_{\mathrm{d}}T_{\mathrm{s}}})|$ of the two methods with changes of ω_{o}, k_{rc} and Q, K.

Fig. 6, where the controller $G_{\mathrm{h}}(z)$ of the composite ADRC in Fig. 1 is also chosen as the repetitive controller [22]. As can be seen from Fig. 6, compared with the composite ADRC, the values of $|G_{\mathrm{d}}(\mathrm{e}^{\mathrm{j}\omega_{\mathrm{d}}T_{\mathrm{s}}})|$ of the proposed ADRC are smaller at frequencies around $6n\omega_{\mathrm{e}}$. It indicates that the proposed ADRC can effectively suppress the $6n$th periodic disturbances caused by the deadtime effect and flux harmonics in the current loop.

According to (8), (10), (13), (26), and (29), it can be seen that the values of $|G_{\mathrm{d}}(\mathrm{e}^{\mathrm{j}\omega_{\mathrm{d}}T_{\mathrm{s}}})|$ of both proposed ADRC and composite ADRC are related to parameters ω_{o}, k_{rc}, Q, and K. To compare the suppression performances of the two methods for periodic disturbances, Fig. 7 describes the values of $|G_{\mathrm{d}}(\mathrm{e}^{\mathrm{j}\omega_{\mathrm{d}}T_{\mathrm{s}}})|$ of the two methods with changes of ω_{o}, k_{rc} and Q, K. The disturbance frequency $\omega_{\mathrm{d}} = 6\omega_{\mathrm{e}}$ is chosen to be 1507 rad/s (the speed is 600 r/min). As can be seen, compared with the composite ADRC, the values of $|G_{\mathrm{d}}(\mathrm{e}^{\mathrm{j}\omega_{\mathrm{d}}T_{\mathrm{s}}})|$ of the proposed

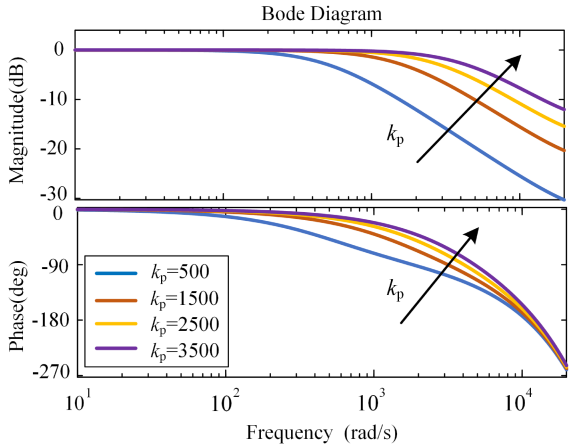

Fig. 8. Bode diagrams of the transfer function $G_{\mathrm{t}}(z)$ with different values of k_{p}.

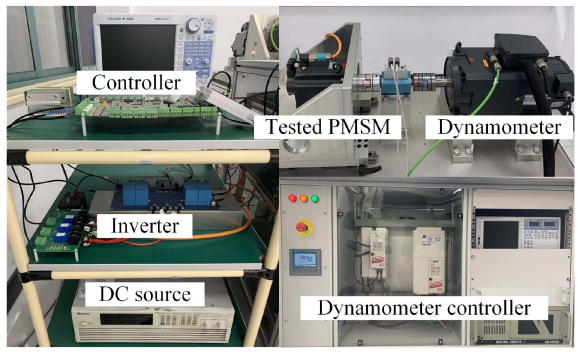

Fig. 9. Experimental platform.

ADRC are smaller in the ranges of ω_{o}, k_{rc}, Q and K, which fully illustrates the superiority of the proposed method for the periodic disturbance rejection.

3) Reference Tracking Performance: As can be seen from (18), since the proposed ADRC method has the decoupling characteristic, the reference tracking performance of the system is only affected by the proportional coefficient k_{p} of the control law, not the structure design and parameter selection of the IESO. Fig. 8 shows Bode diagrams of the transfer function $G_{\mathrm{t}}(z)$ with different values of k_{p}. As can be seen, the transfer function $G_{\mathrm{t}}(z)$ is equivalent to a first-order low-pass filter. It indicates that the proposed ADRC based on the designed IESO can track the reference commands without steady-state errors.

V. Experimental Results

To verify the feasibility and validity of the proposed method, the experiments are carried out on a 3.1-kW surface-mounted PMSM drive system. Fig. 9 is the photograph of the experimental platform, and the parameters of the tested PMSM are given in Table I. The control system's sampling frequency and carrier frequency are 10 kHz. The deadtime of the inverter is 1 μs. In the following experiments, the PMSM current control algorithms based on the proposed two-degree-of-freedom ADRC,

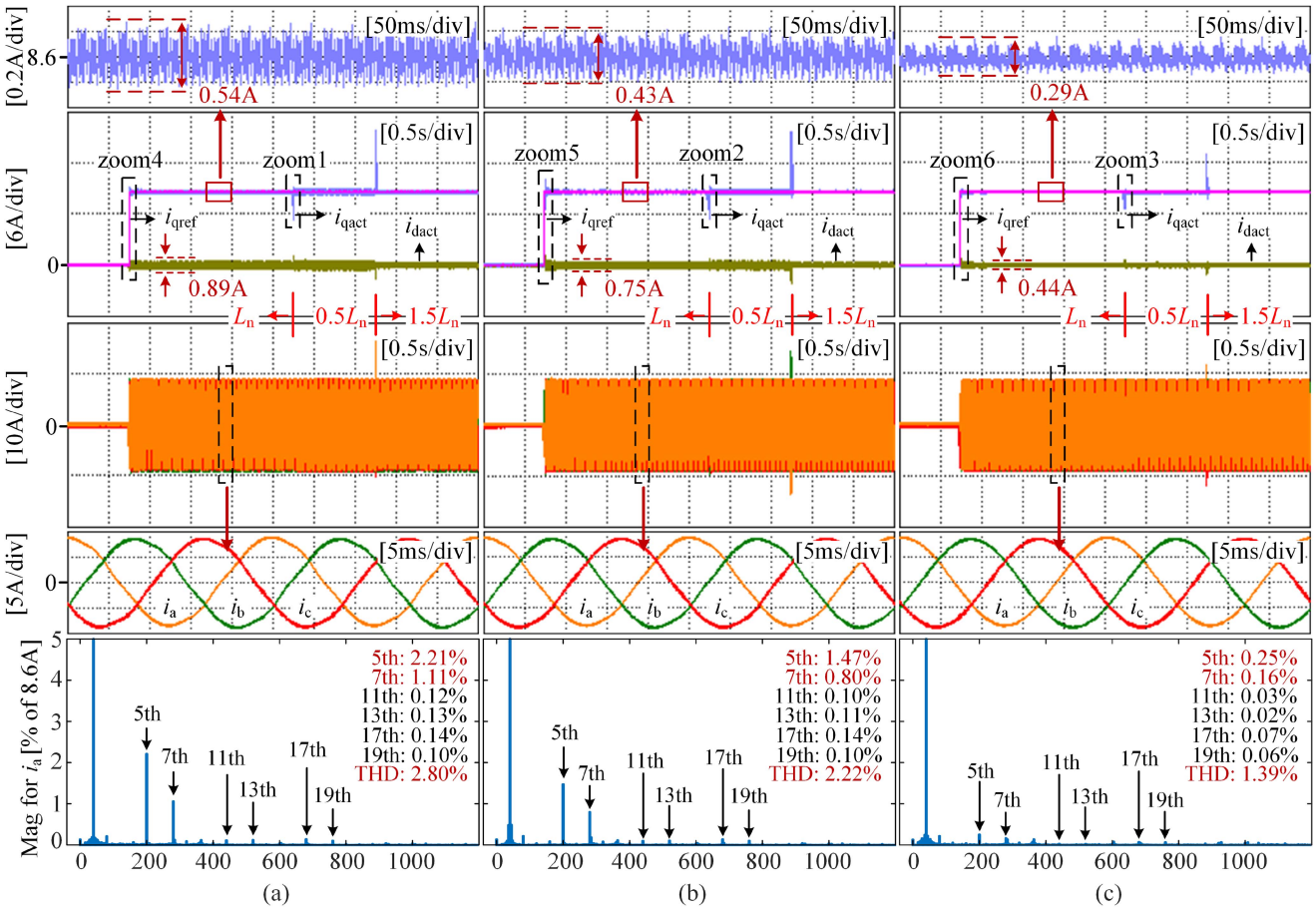

Fig. 10. Overall experimental results of d- and q-axes currents and the phase current harmonic contents. (a) Conventional ADRC. (b) Composite ADRC. (c) Proposed ADRC.

TABLE I
PARAMETERS OF PMSM

Parameter	Value	Parameter	Value
Rated power P_n	3.1 kW	Pole pairs	4
Rated torque T_n	15 Nm	Stator inductance L_n	8 mH
Rated speed n_n	2000 r/min	Stator resistance R_n	0.58 Ω
Total inertia J_n	0.031 kgm^2	Flux linkage ψ_{rn}	0.292 Wb

the conventional ADRC, and the composite ADRC [22] are implemented, respectively.

A. Comparisons of Disturbance Rejection Performance and Reference Tracking Performance

Fig. 10 shows the overall experimental results of the current control with three different control methods. The parameter values of d- and q-axes current controllers of the three methods are the same as those in Fig. 6. The experimental conditions are as follows. First, the q-axis current reference i_{qref} step changes from 0 to 8.6 A (the q-axis rated current), after 2 s, the inductance of the controller step changes from L_n to $0.5\,L_n$, and after 1 s, the inductance of the controller step changes from $0.5\,L_n$ to $1.5\,L_n$. The d-axis current reference i_{dref} is set to 0 A. The speed reference is set to 600 r/min. In these figures, i_{dact} and i_{qact} are d- and q-axes actual currents, respectively. It should be noted that since contents of the $6n$th harmonics of d- and q-axes currents can be reflected through the $(6n\pm1)$th harmonics of phase currents, harmonic contents of the A phase current are analyzed for simplicity in this article.

1) Periodic Disturbance Suppression: As can be seen from Fig. 10(a), with the conventional ADRC method, the periodic disturbances caused by the deadtime effect and flux harmonics cannot be effectively suppressed so that the steady-state control performance of the current deteriorates. The phase current contains numerous fifth and seventh harmonics, which are 2.21% and 1.11%, respectively. The phase current's total harmonic distortion rate (THD) is 2.80%. Moreover, the fluctuations of d- and q-axes steady-state currents are large, which are 0.89 and 0.54 A, respectively. As can be seen from Fig. 10(b), with the composite ADRC method, by optimizing the control law, the periodic disturbances can be suppressed to a certain extent, and the steady-state control performance of the current is improved. The contents of the fifth and seventh harmonics of the phase current are 1.47% and 0.80%, respectively. The THD of the phase current is 2.22%. The fluctuations of d- and q-axes steady-state currents are 0.75 and 0.43 A, respectively. As

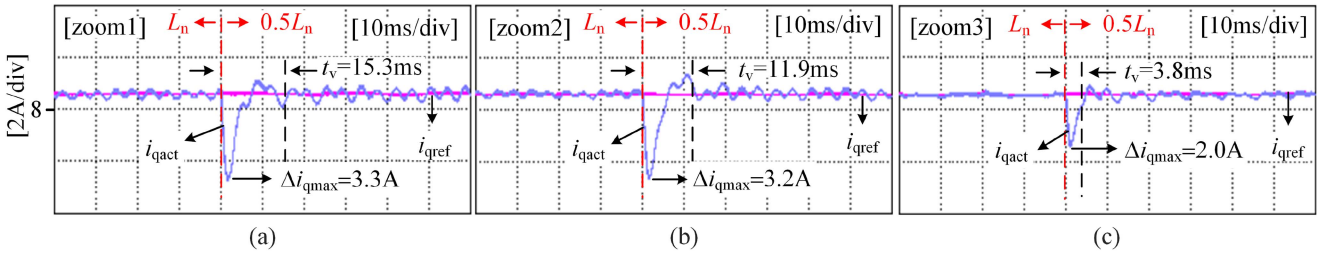

Fig. 11. Zoomed waveforms under the inductance step change. (a) Conventional ADRC. (b) Composite ADRC. (c) Proposed ADRC.

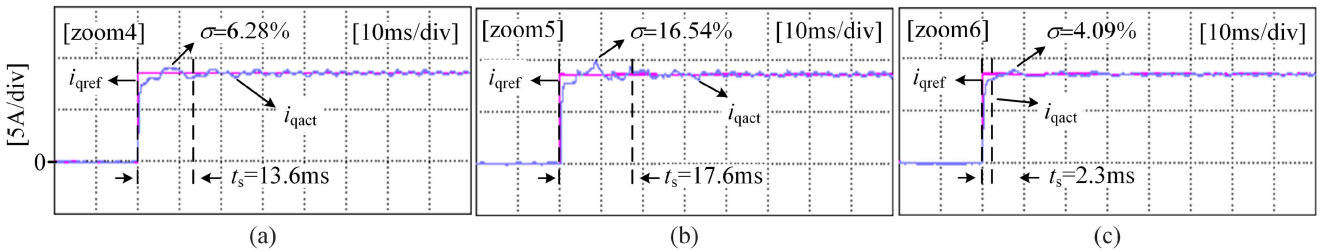

Fig. 12. Zoomed waveforms under the q-axis current reference step change. (a) Conventional ADRC. (b) Composite ADRC. (c) Proposed ADRC.

can be seen from Fig. 10(c), with the proposed ADRC method, the steady-state control performance of the current is improved significantly due to the effective suppression of periodic disturbances. The contents of the fifth and seventh harmonics of the phase current are 0.25% and 0.16%, respectively. The THD of the phase current is 1.39%. The fluctuations of d- and q-axes steady-state currents are 0.44 and 0.29 A, respectively, which reduce by 50.6% and 46.3% compared with the conventional ADRC method, as well as 41.3% and 32.6% compared with the composite ADRC method.

Comparing the steady-state experimental results of the three control methods illustrates that the proposed method can effectively suppress periodic disturbances and improve the steady-state control accuracy of d- and q-axes currents. Moreover, compared with the composite method, the proposed method has a stronger rejection performance for periodic disturbances, which is consistent with the theoretical analysis in Section IV-D.

2) Aperiodic Disturbance Suppression: According to (4), the stator resistance voltage drop, cross-coupling terms, and the inductance mismatches are regarded as aperiodic disturbances, estimated and feedforward compensated by the disturbance observer. As can be seen from Fig. 10(c), with the proposed ADRC method, the excellent current control performance can be achieved no matter the q-axis current reference step changes or the inductance step changes. It indicates that the proposed method can effectively suppress aperiodic disturbances.

Fig. 11 shows the zoomed waveforms of the q-axis current of three control methods when the inductance step changes to demonstrate the superiority of the proposed method for the aperiodic disturbance rejection. As can be seen, with the proposed ADRC method, the maximum drop value $\Delta i_{q\max}$ and the recovery time[1] t_v of the q-axis current are the smallest, which are 2.0 A and 3.8 ms, respectively. It indicates that the proposed method has a stronger suppression performance for aperiodic disturbances. According to Fig. 6, the reason is that the transfer function $G_d(z)$ of the proposed method has a smaller value at the same disturbance frequency.

3) Reference Tracking: Fig. 12 shows the zoomed waveforms of the q-axis current of three control methods when the q-axis current reference step changes. The reference tracking performances of the three control methods are compared by analyzing the overshoot σ and the settling time[2] t_s. As can be seen from Fig. 12, the composite ADRC has the largest values of σ and t_s, which are 16.54% and 17.6 ms, respectively, while the proposed ADRC has the smallest values of σ and t_s, which are 4.09% and 2.3 ms, respectively. It indicates that the proposed method has a better reference tracking performance.

4) Disturbance Compensation: To verify that the output of the designed IESO can simultaneously compensate for periodic and aperiodic disturbances, Fig. 13 shows the experimental results of the d- and q-axes reference voltages and the disturbance compensation components of the proposed ADRC and composite ADRC, respectively. The experimental conditions in Fig. 13 are identical to those in Fig. 10. As can be seen from Fig. 13(a), with the composite ADRC, the aperiodic disturbance compensation components in the d- and q-axes reference voltages are mainly estimated by the ESO, while the periodic disturbance compensation components are the outputs of the repetitive controller. As can be seen from Fig. 13(b), different from the composite ADRC, with the proposed ADRC, aperiodic

[1]Recovery time: The shortest time from the start of the step change of the inductance until the difference between the q-axis actual current and current reference has been kept within the range $\pm 5\%$ of the q-axis current reference.

[2]Settling time: The shortest time from the start of the step change of the q-axis current reference until the difference between the q-axis actual current and current reference has been kept within the range $\pm 5\%$ of the step value.

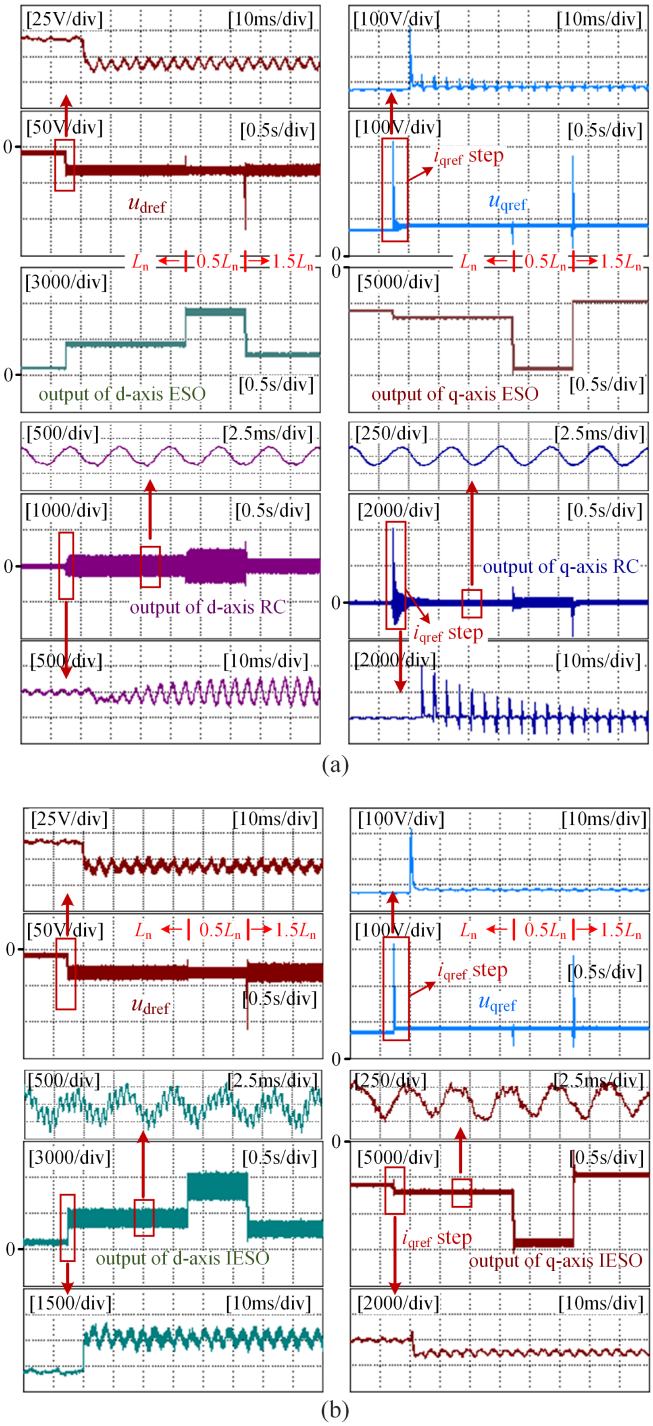

Fig. 13. Experimental results of d- and q-axes reference voltages and the disturbance compensation components. (a) Composite ADRC. (b) Proposed ADRC.

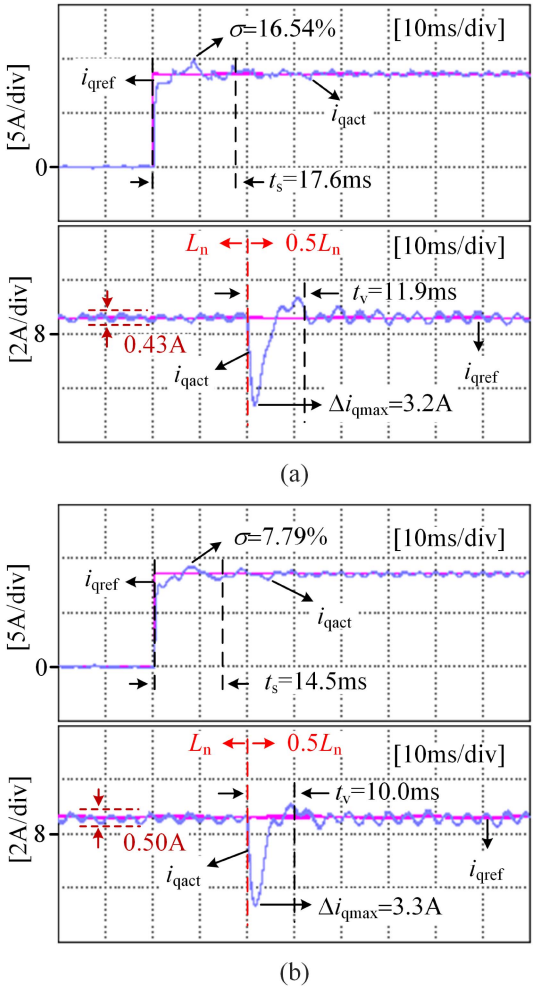

Fig. 14. Experimental results with parameter values of the composite ADRC controller change at 600 r/min. (a) $k_p = 2500$, $Q = 0.95$, $k_{rc} = 500$. (b) $k_p = 2500$, $Q = 0.8$, $k_{rc} = 100$.

and periodic disturbance compensation components in the d- and q-axes reference voltages are both estimated by the designed IESO.

Moreover, as can be seen from the zoomed waveforms of the q-axis reference voltage and the q-axis repetitive controller output of the composite method in Fig. 13(a), although the output of the repetitive controller in the composite control law can suppress the periodic disturbances, when the q-axis current reference step changes, the output oscillation of the q-axis repetitive controller will result in the large oscillation amplitude of the q-axis reference voltage output, so as to deteriorate the system's reference tracking performance. As can be seen from the zoomed waveforms of the q-axis reference voltage and the q-axis IESO output of the proposed method in Fig. 13(b), when the q-axis current reference step changes, the output of the q-axis IESO will not result in the large oscillation amplitude of the q-axis reference voltage output. Therefore, the proposed method has a better reference tracking performance.

B. Decoupling Characteristic Verification

1) Coupling Characteristic of Composite ADRC: Fig. 14 shows the experimental results of the q-axis current at 600 r/min when the parameters of the composite ADRC controller change. As can be seen, when parameters Q and k_{rc} of the repetitive controller in the control law reduce from 0.95 and 500 to 0.8 and 100, respectively, the overshoot σ and the settling time t_s of the q-axis current reduce from 16.54% and 17.6 ms to 7.79%

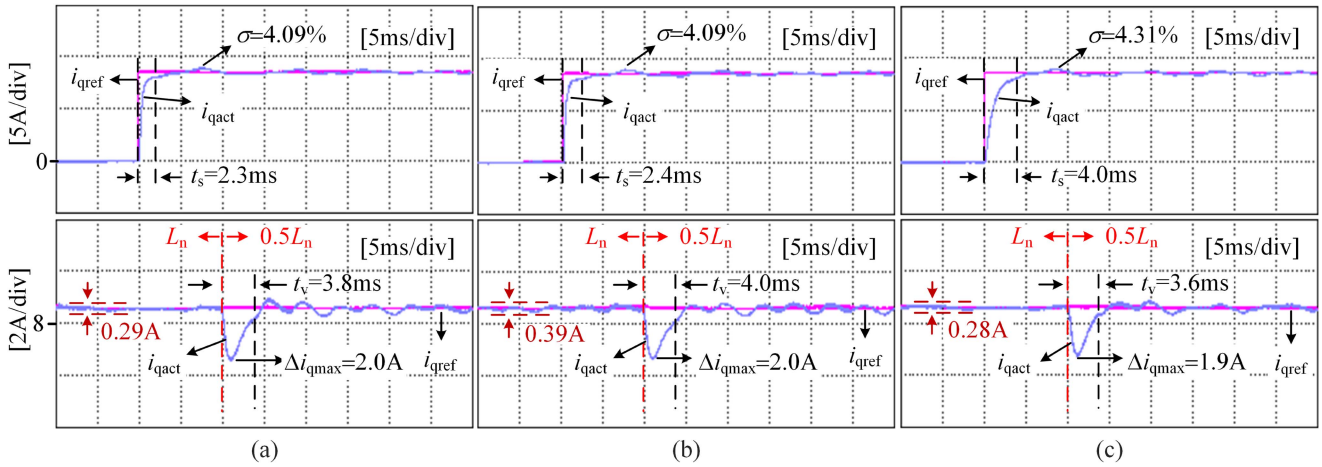

Fig. 15. Experimental results with parameter values of the proposed ADRC controller change at 600 r/min. (a) $k_p = 2500$, $Q = 0.95$, $k_{rc} = 500$. (b) $k_p = 2500$, $Q = 0.8$, $k_{rc} = 100$. (c) $k_p = 1000$, $Q = 0.95$, $k_{rc} = 500$.

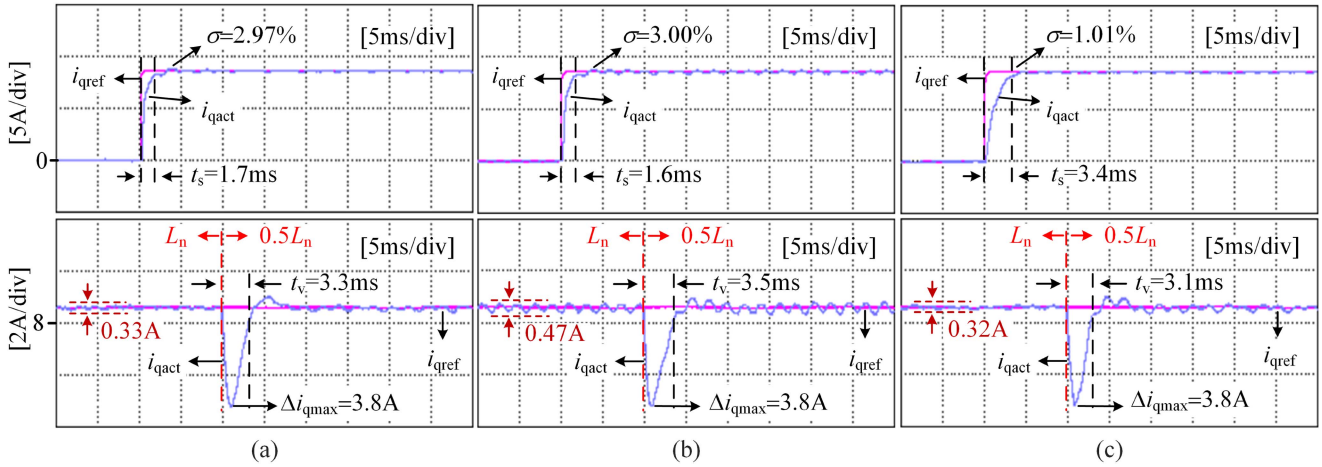

Fig. 16. Experimental results with parameter values of the proposed ADRC controller change at 1200 r/min. (a) $k_p = 2500$, $Q = 0.95$, $k_{rc} = 500$. (b) $k_p = 2500$, $Q = 0.8$, $k_{rc} = 100$. (c) $k_p = 1000$, $Q = 0.95$, $k_{rc} = 500$.

and 14.5 ms, respectively. The reference tracking performance of the system is improved. However, reducing Q and k_{rc} also weakens the rejection performance for periodic disturbances, increasing the q-axis steady-state current fluctuation from 0.43 to 0.50 A. The above analysis indicates that the reference tracking performance and disturbance suppression performance of the composite ADRC method are coupled with each other, which means that neither of these performances can be improved independently by tuning the controller's parameters, and a tradeoff is needed.

2) Decoupling Characteristic of Proposed ADRC: Fig. 15 shows the experimental results of the q-axis current at 600 r/min when the parameters of the proposed ADRC controller change. By comparing Fig. 15(a) and (b), it can be seen that when parameters Q and k_{rc} of the IESO reduce from 0.95 and 500 to 0.8 and 100, respectively, the q-axis steady-state current fluctuation increases from 0.29 to 0.39 A, while the overshoot σ and the settling time t_s are basically unchanged. It illustrates that changing the parameters of the IESO will only affect the disturbance suppression performance but not the reference tracking performance. Moreover, by comparing Fig. 15(a) and (c), it can be seen that when the parameter k_p of the control law reduces from 2500 to 1000, the settling time t_s of the q-axis current increases from 2.3 to 4.0 ms, while the steady-state fluctuation, the maximum drop value $\Delta i_{q\max}$, and the recovery time t_v are basically unchanged. It illustrates that changing the control law parameter will only affect the reference tracking performance but not the disturbance suppression performance.

To fully verify the decoupling characteristic of the proposed method, Fig. 16 shows the experimental results of the q-axis current at 1200 r/min when the parameters of the proposed ADRC controller change. By comparing Fig. 16(a) and (b), it can be seen that when parameters Q and k_{rc} of the IESO reduce from 0.95 and 500 to 0.8 and 100, respectively, the q-axis steady-state current fluctuation increases from 0.33 to 0.47 A, while the overshoot σ and the settling time t_s are basically unchanged. It illustrates that changing the parameters of the IESO will only affect the disturbance suppression performance but not

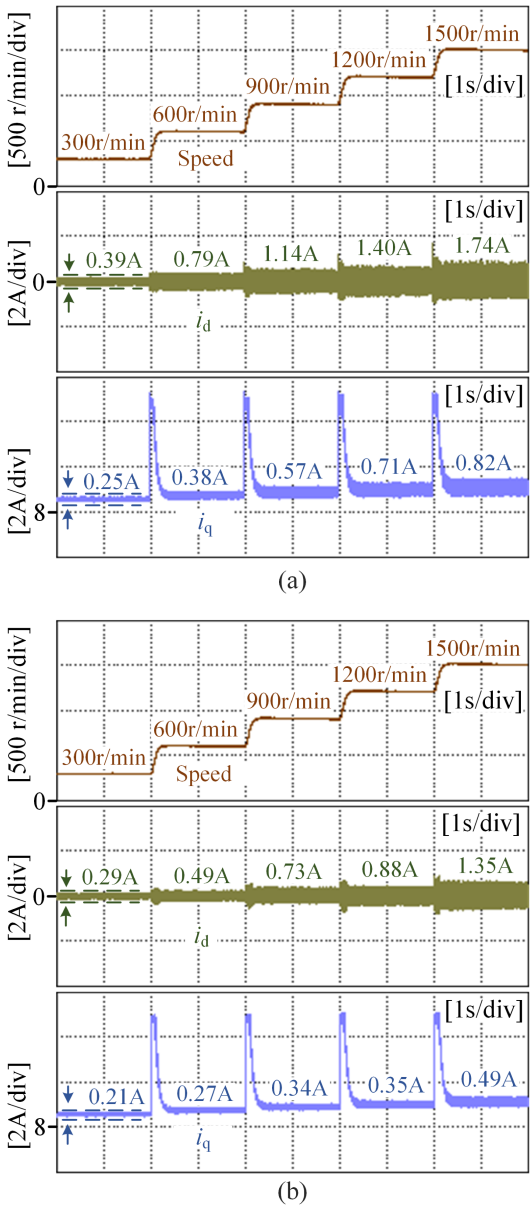

Fig. 17. Experimental results with the speed reference change under the rated load torque. (a) Composite ADRC. (b) Proposed ADRC.

the reference tracking performance. Moreover, by comparing Fig. 16(a) and (c), it can be seen that when the parameter k_p of the control law reduces from 2500 to 1000, the settling time t_s of the q-axis current increases from 1.7 to 3.4 ms, and the overshoot σ of the q-axis current reduces from 2.97% to 1.01%, while the steady-state fluctuation, the maximum drop value $\Delta i_{q\max}$ and the recovery time t_v are basically unchanged. It illustrates that changing the control law parameter will only affect the reference tracking performance but not the disturbance suppression performance.

These two sets of experimental results fully verify that the proposed ADRC controller is a two-degree-of-freedom controller, which means that the reference tracking performance and disturbance suppression performance can be improved simultaneously by tuning parameters of the control law and IESO, respectively. It is advantageous to achieve the excellent current control with the high dynamic response and high steady-state precision.

C. Comparison of Control Performance at Different Speeds

To verify the feasibility and superiority of the proposed ADRC current control method at different speeds, Fig. 17 shows the experimental results of the proposed method and composite method when the speed reference changes from 300 up to 1500 r/min under the rated load torque. As can be seen, the proposed ADRC current control method can operate excellently at different speeds. In addition, compared with the composite ADRC current control method, the fluctuation amplitudes of both d- and q-axes currents of the proposed method are smaller, which indicates that the proposed method has better current control performance at different speeds.

VI. Conclusion

To fully decouple the system's reference tracking performance and disturbance rejection performance, a two-degree-of-freedom ADRC current control method based on the IESO is proposed in this article. The proposed method can simultaneously optimize the reference tracking performance and disturbance rejection performance by independently tuning parameters of the control law and IESO. In practical applications, the proposed method does not need the tradeoff between the two performances, which reduces the complexity of controller parameter tuning. The stability and control performance of the proposed method are analyzed in detail in the discrete-time domain, and a two-step parameter tuning guideline of the IESO is provided to further reduce the complexity of controller parameter tuning. The experimental investigations demonstrate that compared with the conventional ADRC and composite ADRC current control methods, the proposed method optimizes not only the tracking performance for reference commands but also the suppression performance for periodic and aperiodic disturbances. The proposed method simultaneously improves the current control's dynamic response speed and steady-state control accuracy, which is advantageous to achieve the excellent operation performance of PMSM servo systems. Due to the generality of the proposed two-degree-of-freedom ADRC method, it can be applied to other industrial fields in the future.

References

[1] C. Xia, N. Liu, Z. Zhou, Y. Yan, and T. Shi, "Steady-state performance improvement for LQR-based PMSM drives," *IEEE Trans. Power Electron.*, vol. 33, no. 12, pp. 10622–10632, Dec. 2018.

[2] Z. Tang and B. Akin, "A new LMS algorithm based deadtime compensation method for PMSM FOC drives," *IEEE Trans. Ind. Appl.*, vol. 54, no. 6, pp. 6472–6484, Nov./Dec. 2018.

[3] C. Gong, Y. Hu, M. Ma, L. Yan, J. Liu, and H. Wen, "Accurate FCS model predictive current control technique for surface-mounted PMSMs at low control frequency," *IEEE Trans. Power Electron.*, vol. 35, no. 6, pp. 5567–5572, Jun. 2020.

[4] Y. Xu, S. Li, and J. Zou, "Integral sliding mode control based deadbeat predictive current control for PMSM drives with disturbance rejection," *IEEE Trans. Power Electron.*, vol. 37, no. 3, pp. 2845–2856, Mar. 2022.

[5] H. Jingqing, "Auto-disturbances-rejection controller and its applications," *Control Decis.*, vol. 1, pp. 19–23, 1998.

[6] J. Han, "From PID to active disturbance rejection control," *IEEE Trans. Ind. Electron.*, vol. 56, no. 3, pp. 900–906, Mar. 2009.
[7] J. Li, H.-P. Ren, and Y.-R. Zhong, "Robust speed control of induction motor drives using first-order auto-disturbance rejection controllers," *IEEE Trans. Ind. Appl.*, vol. 51, no. 1, pp. 712–720, Jan./Feb. 2015.
[8] J. Li, X. Qi, Y. Xia, and Z. Gao, "On asymptotic stability for nonlinear ADRC based control system with application to the ball-beam problem," in *Proc. Amer. Control Conf.*, 2016, pp. 4725–4730.
[9] Z. Gao, "Scaling and bandwidth-parameterization based controller tuning," in *Proc. Amer. Control Conf.*, 2003, pp. 4989–4996.
[10] Q. Zheng, L. Q. Gaol, and Z. Gao, "On stability analysis of active disturbance rejection control for nonlinear time-varying plants with unknown dynamics," in *Proc. 46th IEEE Conf. Decis. Control*, 2007, pp. 3501–3506.
[11] J. Li, Y. Xia, X. Qi, and Z. Gao, "On the necessity, scheme, and basis of the linear–nonlinear switching in active disturbance rejection control," *IEEE Trans. Ind. Electron.*, vol. 64, no. 2, pp. 1425–1435, Feb. 2017.
[12] Z. Hao et al., "Linear/Nonlinear active disturbance rejection switching control for permanent magnet synchronous motors," *IEEE Trans. Power Electron.*, vol. 36, no. 8, pp. 9334–9347, Aug. 2021.
[13] Y. Zuo, X. Zhu, L. Quan, C. Zhang, Y. Du, and Z. Xiang, "Active disturbance rejection controller for speed control of electrical drives using phase-locking loop observer," *IEEE Trans. Ind. Electron.*, vol. 66, no. 3, pp. 1748–1759, Mar. 2019.
[14] L. Qu, W. Qiao, and L. Qu, "An enhanced linear active disturbance rejection rotor position sensorless control for permanent magnet synchronous motors," *IEEE Trans. Power Electron.*, vol. 35, no. 6, pp. 6175–6184, Jun. 2020.
[15] A. M. Diab, S. S. Yeoh, S. Bozhko, C. Gerada, and M. Galea, "Enhanced active disturbance rejection current controller for permanent magnet synchronous machines operated at low sampling time ratio," *IEEE J. Emerg. Sel. Topics Ind. Electron.*, vol. 3, no. 2, pp. 230–241, Apr. 2022.
[16] L. Qu, W. Qiao, and L. Qu, "Active-disturbance-rejection-based sliding-mode current control for permanent-magnet synchronous motors," *IEEE Trans. Power Electron.*, vol. 36, no. 1, pp. 751–760, Jan. 2021.
[17] Y. A.-R. I. Mohamed, "A newly designed instantaneous-torque control of direct-drive PMSM servo actuator with improved torque estimation and control characteristics," *IEEE Trans. Ind. Electron.*, vol. 54, no. 5, pp. 2864–2873, Oct. 2007.
[18] Z. Zhou, C. Xia, Y. Yan, Z. Wang, and T. Shi, "Disturbances attenuation of permanent magnet synchronous motor drives using cascaded predictive-integral-resonant controllers," *IEEE Trans. Power Electron.*, vol. 33, no. 2, pp. 1514–1527, Feb. 2018.
[19] M. Tang, A. Formentini, S. A. Odhano, and P. Zanchetta, "Torque ripple reduction of PMSMs using a novel angle-based repetitive observer," *IEEE Trans. Ind. Electron.*, vol. 67, no. 4, pp. 2689–2699, Apr. 2020.
[20] A. A. Godbole, J. P. Kolhe, and S. E. Talole, "Performance analysis of generalized extended state observer in tackling sinusoidal disturbances," *IEEE Trans. Control Syst. Technol.*, vol. 21, no. 6, pp. 2212–2223, Nov. 2013.
[21] A. H. M. Sayem, Z. Cao, and Z. Man, "Model free ESO-based repetitive control for rejecting periodic and aperiodic disturbances," *IEEE Trans. Ind. Electron.*, vol. 64, no. 4, pp. 3433–3441, Apr. 2017.
[22] M. Tian, B. Wang, Y. Yu, Q. Dong, and D. Xu, "Discrete-time repetitive control-based ADRC for current loop disturbances suppression of PMSM drives," *IEEE Trans. Ind. Inform.*, vol. 18, no. 5, pp. 3138–3149, May 2022.
[23] Z. Wang, J. Zhao, L. Wang, M. Li, and Y. Hu, "Combined vector resonant and active disturbance rejection control for PMSLM current harmonic suppression," *IEEE Trans. Ind. Inform.*, vol. 16, no. 9, pp. 5691–5702, Sep. 2020.
[24] K. Ogata, *Discrete-Time Control Systems*. Englewood Cliffs, NJ, USA: Prentice-Hall, 1995, ch.4.

Shiyu Lin (Student Member, IEEE) was born in Sichuan, China, in 1996. He received the B.S. degree in electrical engineering from Dalian Maritime University, Dalian, China, in 2018. He is currently working toward the Ph.D. degree in electrical engineering with the College of Electrical Engineering, Zhejiang University, Hangzhou, China.

His research interests include electrical machines, servo motor drives, and power electronics.

Yanfei Cao (Member, IEEE) was born in Hebei, China, in 1990. She received the B.S. degree in automation from the Hebei University of Technology, City College, Tianjin, China, in 2013, and the M.S. and Ph.D. degrees in control science and engineering from Tianjin University, Tianjin, China, in 2019.

She is currently an Associate Researcher with the College of Electrical Engineering, Zhejiang University, Zhejiang, China. Her research interests include electrical machines, motor drives, and power electronics.

Chen Li was born in Shandong, China, in 1991. He received the B.S. degree from the China University of Mining and Technology, Jiangsu, China, in 2014, and the Ph.D. degree from Tianjin University, Tianjin, in 2022, both in electrical engineering.

He is currently a Postdoctoral Researcher with the Zhejiang University Advanced Electrical Equipment Innovation Center, Hangzhou, China. His current research interests include electrical machines, motor drives, and power electronics.

Zhiqiang Wang (Member, IEEE) was born in Tianjin, China, in 1984. He received the B.S. degree from the Hebei University of Technology, Tianjin, China, in 2006, and the M.S. and Ph.D. degrees from Tianjin University, China, in 2008 and 2012, all in electrical engineering, respectively.

He is currently an Associate Professor in the School of Electrical Engineering, Tiangong University, Tianjin, China. His research interests include power electronics technology and intelligent control of motor systems.

Tingna Shi (Member, IEEE) was born in Yuyao, China, in 1969. She received the B.S. and M.S. degrees from Zhejiang University, Hangzhou, China, in 1991 and 1996, respectively, and the Ph.D. degree from Tianjin University, Tianjin, China, in 2009, all in electrical engineering.

She is currently a Professor with the College of Electrical Engineering, Zhejiang University. Her current research interests include electrical machines and their control systems, power electronics, and electric drives.

Changliang Xia (Senior Member, IEEE) was born in Tianjin, China, in 1968. He received the B.S. degree from Tianjin University, Tianjin, China, in 1990, and the M.S. and Ph.D. degrees from Zhejiang University, Hangzhou, China, in 1993 and 1995, respectively, all in electrical engineering.

He was a Full Professor with the School of Electrical Engineering and Automation, Tianjin University, in 2002. Since 2018, he has been the President of Tiangong University, Tianjin, China, where he is currently a Full Professor and the Director of the National Local Joint Engineering Research Center of Electrical System Design and Manufacturing. He also serves as the Qiushi Chair Professor of Zhejiang University. He has authored or coauthored more than 200 journal papers, four books, and 60 patents. His research interests include electrical machines, power electronics, and their control systems.

Dr. Xia was elected as an Academician of the Chinese Academy of Engineering in 2017. He was the recipient of the State Science and Technology Awards of China twice.